Low Frequency Ultrasound Enhanced Dual Amination of Biochar: A Nitrogen-Enriched Sorbent for CO₂ Capture

Riya Chatterjee, Baharak Sajjadi, Wei-Yin Chen, Daniell L. Mattern, Nosa O. Egiebor, Alexander Nosa O. Egiebor, Nathan Hammer, [‡] and Vijayasankar Raman

ABSTRACT: The present study discusses a novel biochar activation technique consisting of physical modification using low frequency ultrasound and chemical functionalization with individual amines and their blended mixtures in the presence of two activating agents. Acoustic treatment under ultrasonic irradiation exfoliates the biochar's graphitic clusters, creates new micropores, opens the blocked pores, and enhances the functionalization efficiency. In a subsequent chemical modification step, functionalization with amine moieties further boosts the adsorption capacity. Therefore, the effect of five different amines was investigated on ultrasono-activated biochar (i) monoethanolamine (MEA, 1°), (ii) piperazine (PZ, 2°), (iii) diethanolamine (DEA, 2°), (iv) tetraethylenepentamine (TEPA, 1° and 2°), and (v) polyethylenimine (PEI, 1°, 2°, and 3°) and several binary and ternary mixtures (1) MEA-TEPA, (2) DEA-TEPA, (3) DEA-PEI, (4) TEPA-PEI, and (5) DEA-TEPA-PEI with the activating agents N-(3-(dimethylamino)propyl-N'-ethylcarbodiimide hydrochloride (EDC)-hydroxybenzotriazole (HOBt) or potassium hydroxide (KOH). The results revealed that ultrasonically treating biochar samples for 30 s, followed by chemical activation with either EDC-HOBt-TEPA-MEA or KOH-MEA gave materials possessing intensified adsorption capacities of 1.91 and 1.62 mmol/g, respectively, at 0.10 atm CO₂ partial pressure and 70 °C, compared to raw biochar (0.3 mmol/g).

1. INTRODUCTION

Downloaded via UNIV OF MISSISSIPPI on March 14, 2019 at 18:27:48 (UTC). See https://pubs.acs.org/sharingguidelines for options on how to legitimately share published articles.

Amination of carbonaceous materials has received significant attention because of the following applications-enhanced adsorption of pollutants (such as Ni, Cd, methylene blue, and ibuprofen), manufacturing of carbon quantum dots, site specific drug delivery,³ etc.—and specifically for CO₂ capture. Amines (used as sorbents in the amination technique) as a nucleophile have strong affinity for CO2 (electrophilic) and can interact through nucleophilic addition.⁴ Aqueous amine scrubbing has proven to increase the CO₂ absorption rate.⁵ However, the regeneration process is energy intensive because of the high specific heat of aqueous amines. To overcome this drawback, CO₂ adsorption with solid sorbents is emerging as an efficient and economic technique because of the low heat capacity, high thermal stability, and no corrosion problems of solids. Moreover, the sorbents have tunable pore size and surface area and are synthesized from readily available feedstocks. Additionally, the presence of effective oxygen functional groups facilitates the attachment of nitrogenous compounds (such as amines) to further improve the sorption capacity.

Apart from achieving optimized adsorption capacity, regeneration of the adsorbent is equally important from an economic point of view and for its long-term use. The commonly available regeneration techniques are pressure swing adsorption (PSA), vacuum swing adsorption (VSA), temperature swing adsorption (TSA), and electric swing adsorption. In PSA, the pressure is reduced for the desorption since adsorption is done at high pressure, whereas in TSA, the temperature is raised to desorb the adsorbate gas since adsorption is an exothermic process, while desorption is endothermic.8 VSA is the technique where vacuum or below atmospheric pressure is applied for regeneration. Within TSA technologies, the specific case in which the solid is heated by the Joule effect is commonly referred to as ESA.7 Each of the processes has its own importance and pitfalls as mentioned in the following section. PSA does not need elevated temperature, so the energy requirement is low. But to effectively regenerate adsorbent it requires multiple stages which makes the process expensive. Whereas, VSA requires a highly efficient vacuum pump to effectively desorb CO₂, which adds extra costs. 10,11 TSA is very cost-effective and easily operated since it does not need any pumping system, but it needs high volume purge gases to provide heat for regeneration. 10,12 ESA has advantages of less heat requirement and fast kinetics, but its electrical energy consumption is very high.8 Additionally, the regeneration ability of the sorbent was studied in detail in our previous work.4 TSA regeneration tests were conducted at the elevated temperature of 180 °C under helium (He) gas flow for 60 min. The test was conducted 15 times, and the adsorbent was

Received: October 12, 2018 Revised: January 2, 2019 Published: January 10, 2019



[†]Department of Chemical Engineering, School of Engineering, University of Mississippi, 134 Anderson Hall, Mississippi 38677-1848, United States

[‡]Department of Chemistry and Biochemistry, University of Mississippi, Coulter Hall, Mississippi 38677, United States

[§]Environmental Resources Engineering Department, College of Environmental Science and Forestry, 206 Bray Hall, Syracuse, New York 13210, United States

National Center for Natural Products Research, School of Pharmacy, University of Mississippi, University, MS 38677, United States

reused for CO_2 adsorption after each regeneration cycle. The results demonstrated that US0.5-EH1:1-T2.5 could maintain 56% of its initial adsorptive capacity after 15 cycles of adsorption—regeneration.

Additionally, key to enhanced adsorption capacity is effective nitrogenation that depends on the interactions between the functional group (such as amino group) and its support (carbonaceous materials). For instance, the reaction of carbonaceous compounds with ammonia leads to the formation of functional groups such as $-\mathrm{NH}_2$, $-\mathrm{CN}$, pyridine, quaternary nitrogen, imide, and pyrrole-like structures. Another reaction, involving a mixture of nitric and sulfuric acids, creates nitro $(-\mathrm{NO}_2)$ groups through electrophilic aromatic substitution (Figure 1) followed by reduction to amino groups via NaHSO3.

Figure 1. Nitration of carbonaceous compounds.

Among different amination methods, EDC-HOBt coupling or KOH treatments are highly potent methods. The EDC-HOBt reaction (Figure 2) is a one-pot method at room

Figure 2. Amine treatment of carbonaceous compound.

temperature with fast kinetics and ease of product separation. EDC as a coupling agent activates the —COOH group to form O-acyl-isourea followed by nucleophilic substitution by amino groups producing amide and releasing dialkyl-urea as a byproduct. However, it may lead to side reaction through cleaving off the activated ester intermediate (O-acylisourea) forming N-acyl urea. This can be prevented by the addition of HOBt, which forms the intermediate (Figure 2) before the migration.

The alternate route of activation with KOH treatment (prior to amination) is used for metal ion adsorption. ¹⁷ The mechanism may be primarily physical, by causing changes in the porosity and surface area of the char. ¹⁸ Other studies have found evidence for chemical modification of the char, including an increase in oxygen content and a decrease in carbonyl groups. ¹⁷ Simple deprotonation of carboxyl groups by hydroxide would create carboxylates that eventually protonated to carboxylic acids. Besides, opening of epoxides with hydroxide would add hydroxyl-group oxygen to the system

that would allow for amine coordination through hydrogen bonding. KOH changes porosity and decrease oxygen content of biochar under the extreme local temperatures generated during ultrasonication similar to the phenomenon observed under high temperature (850 °C) treatments. ¹⁹ Alternatively, partial breakdown of the biochar carbon skeleton might be assisted by KOH, with air oxidation to more —COOH or —OH sites for interaction with amines.

A major goal of the amination is to achieve maximal amine loading that could be achieved through the amalgamation of two or more amines. Additionally, literature suggests that amine mixtures or blended amines can have higher reaction rates and sorption capacities and lower regeneration temperature than single amine systems. 20 1° and 2° amines can form ammonium bicarbonate salts (requiring only one amine per CO₂) as well as zwitterion-carbamate products (requiring two amines), while 3° amines only form the salt. Therefore, 3° amines have a theoretically higher CO₂ adsorption capacity, but slow kinetics. The present study explores the effect of five different amines (i) monoethanolamine (MEA, 1°), (ii) piperazine (PZ, 2°), (iii) diethanolamine (DEA, 2°), (iv) tetraethylenepentamine (TEPA, 1° and 2°), and (v) polyethylenimine (PEI, 1°, 2°, and 3°) and some binaryternary mixtures MEA-TEPA, DEA-TEPA, DEA-PEI, TEPA-PEI, and DEA-TEPA-PEI, on ultrasonically activated biochar for enhanced CO2 adsorption. The specific characteristics of the different amines are presented in Table 1.

The main objective of a series of our previous studies^{4,21} was to develop an advanced method for activation of carbonaceous structures which can be applied at lower temperatures than conventional carbon activation. To reach this objective, the emphasis has been given on the integration of physicochemical activation processes. The focus of the previous work was on investigating the effect of ultrasound intensity, amine concentration, adsorption temperature, and inlet CO₂ concentration on the adsorption capacity of the activated biochar. The current work investigates the interaction of blended amines in the ultrasonic physical activation technique for its application in CO₂ capture. Ultrasound increases the porosity of the biochar, so a structure with a combination of micro- and mesopores is generated. Such ultrasound-assisted pore generation and surface destructions have wide arrays of applications in several fields, e.g., for water purification to break down pollutants,²² in medicine for the destruction of kidney stones, 23 for targeted drug delivery through modification of the cell plasma membrane,²⁴ etc. The second reason is more related to simplifying the chemical step by eliminating the preactivation using EDC and HOBt and substituting it with KOH. So, based on our previous results^{4,21} and literature reports,²⁰ the present study investigates the effects of different amines and their mixtures, with the aid of low frequency ultrasound energy, to achieve enhanced adsorption capacity of biochar toward CO₂ capture.

2. MATERIALS AND METHODS

2.1. Materials. Pine wood-based biochar, pyrolyzed between 550 and 600 °C in an oxygen-deprived environment in a kiln reactor, was supplied by Biochar Now (Berthoud Colorado, U.S.A.). The reagents used in chemical functionalization, including methanol, *N*-(3-(dimethylamino)propyl-*N*'-ethylcarbodiimide hydrochloride (EDC, 98% purity), hydroxybenzotriazole (HOBt, 97% purity), monoethanolamine (MEA), piperazine (PZ), diethanolamine (DEA), tetraethylenepentamime (TEPA), polyethylenimine (PEI), and potassium hydroxide (KOH) were obtained from Sigma-Aldrich.

Table 1. Structures and Properties of Different Amines

Amine	Structure	Empirical Formula	No. of amine groups	Molecular weight
MonoEthanolAmine	HO NH ₂	C ₂ H ₇ NO	1	61.08
PiperaZine	ZI Z	$C_4H_{10}N_2$	2	86.14
DiEthanolAmine	HO N OH	C ₄ H ₁₁ NO ₂	1	105.14
TetraEthylenePentAmime	$H_2N \sim \stackrel{H}{\stackrel{N}{\sim}} \stackrel{N}{\stackrel{N}{\sim}} \stackrel{N}{\stackrel{N}{\sim}} NH_2$	$C_8H_{23}N_5$	5	189.30
PolyEthylenImine	$\begin{array}{c c} & & & & & & & & & & & & & & & & & & &$	(C ₂ H ₅ N) _n	1 (per repeating - CH ₂ CH ₂ NH - unit)	43.04 (per repeating - CH ₂ CH ₂ NH - unit)

Hydrochloric acid (37%) and acetone were also supplied by Sigma-Aldrich. Sodium hydroxide (NaOH) was obtained from Fisher Scientific. Deionized water was obtained from Milli-Q ultrapure water tap from Millipore Sigma. All chemicals used were of analytical grade.

2.2. Experimental Method. 2.2.1. Functionalization with Ultrasound Treatment of Biochar. Prior to physicochemical modification, raw biochar particles were resized in the range of 75–250 μm by crushing and screening. Physical modification of biochar was then accomplished by low frequency ultrasound (QSonica sonicator model no. Q700), typically with 3 g of biochar in 250 mL of water for 30 s. The duration was selected based on the optimum value obtained from a previous study. Longer duration of sonication promotes intensified cavitation that could disarrange the orientation of the layered structure of biochar, consequently blocking the pores and reducing the adsorption capacity. ^{25,26} The ultrasonically modified biochar was then subjected to chemical modification with simple or blended amines, using either EDC–HOBt or KOH activation. The details of the chemical activation procedures are discussed in the following sections.

2.2.2. Amination of Ultrasonicated Biochar Using EDC-HOBt Activation. First, the ultrasound treated biochar samples were subjected to the coupling agents EDC-HOBt (3.375 g of each coupling agent for 3 g of biochar) in water. EDC was selected as a coupling agent over other carbodiimides, such as dicyclohexylcarbodiimide (DCC), that are sparingly soluble in any solvent, which makes separation very difficult to achieve. HOBt was used as an additive to prevent side reactions that would reduce the yield of products. An equal ratio of EDC and HOBt activates the maximum number of functional groups, as found from our previous study.⁴ The mixture was stirred for 24 h at 35 °C, then filtered and dried under vacuum at 60 °C overnight. In the next step, the dried samples were suspended in methanol (an organic solvent that makes the drying faster). Amines (MEA, PZ, DEA, or PEI) with a weight ratio of 2.5, 5, or 10 times that of biochar were added to the suspension. The resultant mixtures were stirred for 24 h with gentle heating as before. Finally, the suspension was filtered and washed in succession with 200 mL of 1 N NaOH (3 times), 200 mL 1 N HCl (3 times), and 200 mL of acetone (1 time) for each wash and dried as before. For activation with blended amines, the mixtures of MEA-TEPA, DEA-TEPA, DEA-PEI, TEPA-PEI, and DEA-TEPA-PEI were added where the total weight of the mixture was 2.5 times to the weight of the biochar. To achieve this, the loadings of individual amine in binary and ternary mixtures were maintained at 1.25 and 0.83 times to the weight of the biochar, respectively. Thus, the individual amines in the mixture was blended in equal weight ratio (1:1 and 1:1:1 for binary and ternary

mixtures) to give the total weight 2.5 times to the weight of the biochar

2.2.2.1. Amination of Ultrasonicated Biochar Using KOH Activation. Following sonication of the biochar—water mixture as before, KOH (1.5 times the biochar weight) was added to the mixture, which was stirred for 24 h, filtered, and dried under vacuum overnight. The sample was then suspended in methanol, and MEA, PZ, DEA, TEPA, or PEI or their blended mixtures were added as before. All mixtures were kept under stirring for 24 h, filtered, and washed with 1 N NaOH, 1 N HCl, and acetone as before. The dried samples were kept in a desiccator for future CO₂ adsorption tests.

2.3. Characterizations of the Adsorbent. The surface morphology of both raw and activated biochars were examined using SEM (JSM-5600 Scanning Electron Microscope, JEOL USA Inc., Peabody, MS). The effects of ultrasound activation on the surface area and porosity were also investigated by a surface area analyzer (Nova 2000E series, Quantachrome). The elemental compositions of physicochemically modified biochar samples were analyzed before and after modifications (Huffman Hazen Laboratory, Colorado, USA). The surface functional groups of the functionalized biochars were examined using Fourier transform infrared (FTIR, Cary 660 FTIR Agilent). The Raman spectroscopy (LabRam HR Evolution) of the activated samples was conducted for investigating the microstructure of biochar. 27 CO₂ adsorption studies were conducted with 2.5, 5, and 10 times amine loading. However, the adsorption capacities for 5 or 10 times loading were not enhanced substantially compared to the 2.5 times loading. So, the system was optimized with 2.5 times loading and the characterizations were performed only for the 2.5 times loading samples.

2.4. CO₂ Adsorption Studies. The CO₂ adsorption experiments were carried out in a tubular reactor made of alumina oxide. The details of the experimental procedure, and the analysis along with the equation used, were discussed in our previous work.4 In a typical experiment, the functionalized biochar was placed into a temperaturecontrolled furnace inside the reactor. The biochar was degassed with helium gas (99.99%) at a flow rate of 500 cm³/min at 378 K for 1 h, and then cooled to 333 K. The previous work showed that the optimum adsorption capacity was achieved when experiment was conducted at 70 °C temperature compared to 25, 50, and 90 °C. This is due to the chemical activation with amines resulting in chemisorption, which requires high activation energy, hence high temperature. However, the further reduction of adsorption capacity with increasing temperature was attributed to the exothermic nature of the process.²⁸ A similar phenomenon was observed by Heydari-Gorji and Jadhav et al. 28,29 Accordingly, the adsorption temperature of 70 °C was selected for the current study. After setting the

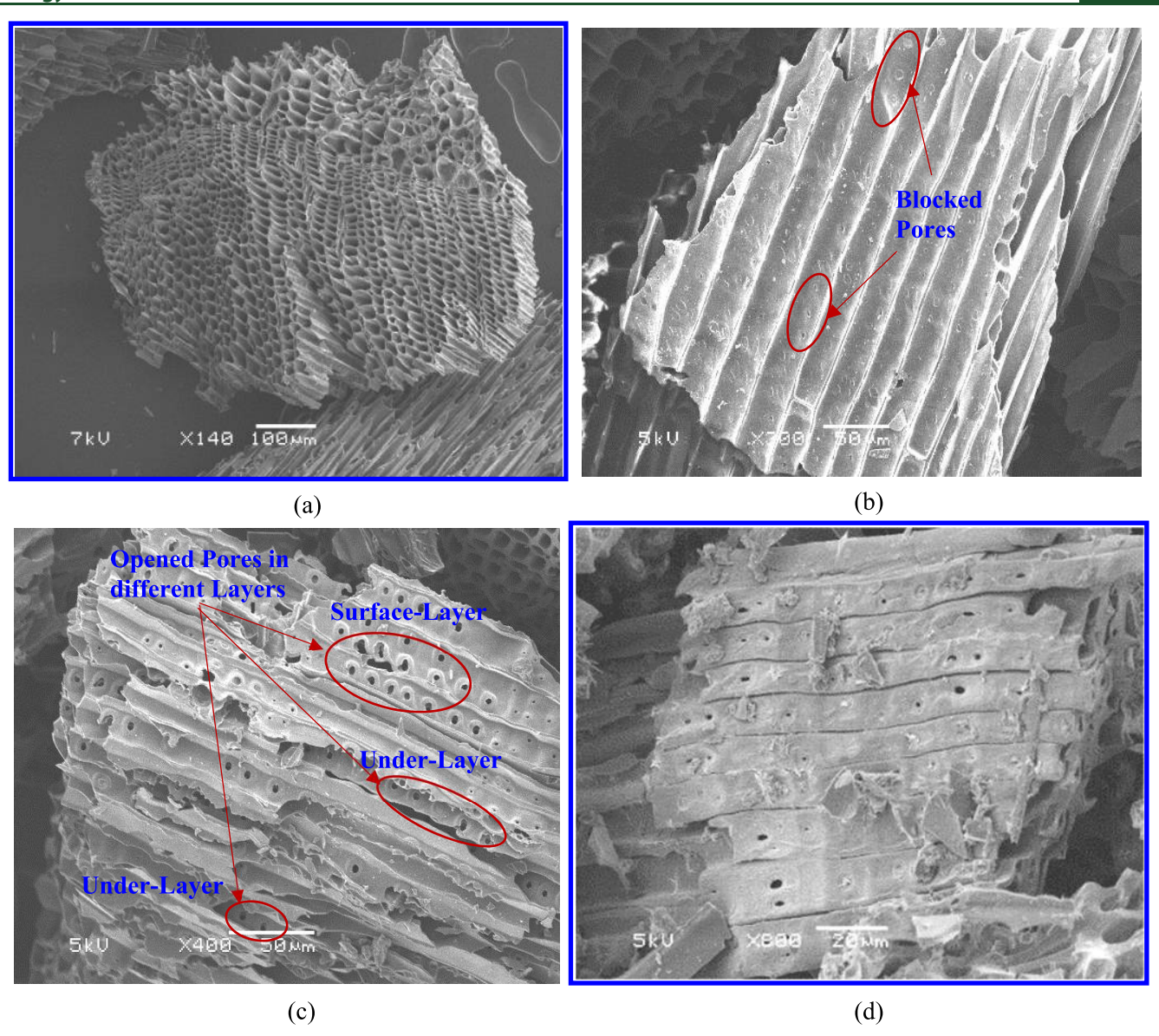


Figure 3. SEM images of (a) raw biochar (cross sectional view), (b) raw biochar (longitudinal view), (c) ultrasound-activated biochar, (d) ultrasound-EDC-HOBt-binary amine (DEA-TEPA) activated biochar US0.5-EH1:1-DT1:1.

temperature at its desired value, the helium flow was switched to a CO_2 -containing simulated flue gas of 10 vol % (balanced with He) at a flow rate of 500 cm³/min. The final concentration of CO_2 after adsorption was measured by a CO_2 analyzer, connected online via the adsorption column outlet. The adsorption capacity was calculated based on the difference between inlet and outlet CO_2 concentrations.

3. RESULTS AND DISCUSSIONS

3.1. Physicochemical Properties of Raw and Modified Biochar Samples. 3.1.1. SEM Analysis. Scanning electron microscopy (SEM) provides information about the surface morphology of a structure. SEM images of raw (both longitudinal and cross-sectional view), ultrasound treated, and EDC-HOBt-binary amine activated (US0.5-EH1:1-DT1:1) are shown in Figures 3a—d. The cross-sectional view (Figure 3a) shows the porous structure of biochar, whereas the longitudinal view (Figure 3b) shows that the raw biochar surface was rough and consisted of blocked pores as shown by the red oval shapes. The observed blockage on the surface can be ascribed to the formation of volatile compounds and ash

(from the mineral matter) during the thermochemical decomposition of the cellular structure of the biomass in pyrolysis.³⁰ The resultant blockage made the surface inaccessible for subsequent chemical modification, lowering the adsorption capacity. However, upon sonication, the surface porosity was enhanced significantly as observed from Figure 3c because of the exfoliation of biochar's graphitic layers and leaching of ash from the pores.³¹ The figure also shows that the ultrasound cavitation was intense enough to create additional porosity not only to the layer adjacent to the surface but also penetrated to the interlayers, breaking the structure and generating pores. This substantially enhanced the surface area of the biochar and facilitated the chemical activation of the underlayers' active sites. In Figure 3d the effect of amination (in the presence of EDC-HOBt activating agents) is portrayed. This image further displays that the surface porous structure as well as the surface were partially covered with amine, which can be further explained as the formation of a coating on the biochar surface.³² This observation is consistent with the surface analysis described in the next section.

Table 2. DR-CO₂ and BET-N₂ Surface Area of Raw Biochar and Physicochemically Activated Biochars^a

	microporosity			micro- and mesoporosity			
sample name	surface area (m²/g)	pore volume (cm ³ /g)	pore radius ⁴⁵	surface area (m²/g)	pore volume(cm ³ /g)	pore radius ⁴⁵	
raw biochar	312.31	0.11	0.58	46.93	0.06	0.80	
US0.5-EH0-A0	395.32	0.12	0.59	22.26	0.03	1.80	
US0.5-EH1:1-M2.5	374.66	0.12	0.57	13.30	0.02	2.80	
US0.5-EH1:1-PZ2.5	172.57	0.06	0.59	1.01	0.004	5.06	
US0.5-EH1:1-D2.5	220.11	0.07	0.63	2.69	0.005	5.04	
US0.5-EH1:1-P2.5	182.04	0.06	0.62	2.01	0.005	5.04	
US0.5-EH1:1-MT1:1	375.12	0.12	0.58	18.16	0.02	2.10	
US0.5-EH1:1-DT1:1	270.96	0.09	0.56	13.30	0.02	2.80	
US0.5-EH1:1-DP1:1	233.46	0.08	0.62	3.41	0.005	4.94	
US0.5-EH1:1-TP1:1	229.05	0.08	0.59	4.54	0.005	4.86	
US0.5-EH1:1-DTP1:1:1	235.62	0.08	0.58	10.14	0.02	3.20	
US0.5-K1.5-M2.5	308.22	0.09	0.55	14.30	0.02	2.92	
US0.5-K1.5-T2.5	298.17	0.09	0.59	16.71	0.02	2.60	
US0.5-K1.5-DT1:1	266.23	0.09	0.61	13.24	0.02	2.80	

"US ultrasound; EH EDC—HOBt; A amine; K KOH; T TEPA; P PEI; D DEA; M MEA; PZ piperazine. The number beside US denotes sonication time in minutes. The number beside EH denotes the ratio of activating agents. The number beside K denotes loading of KOH (weight of KOH to the weight of biochar). The number beside A, T, P, D, M, and PZ denotes amine loading. Numbers beside TD, TP, PD, TM, and TPD denote weight ratio of amines.

Table 3. Elemental Analysis of Raw and Activated Biochars^a

sample	C content (% wt)	H content (% wt)	N content (% wt)	O content (% wt)	ash content (% wt)
raw biochar	65.36	1.97	0.18	11.22	23.95
US0.5-EH1:1-M2.5	64.42	2.43	1.17	13.66	20.50
US0.5-EH1:1-PZ2.5	57.57	2.33	0.38	15.26	27.28
US0.5-EH1:1-D2.5	65.66	2.30	0.58	13.16	21.03
US0.5-EH1:1-P2.5	61.84	2.25	0.46	13.99	23.95
US0.5-EH1:1-MT1:1	66.13	2.54	1.40	16.15	15.66
US0.5-EH1:1-DT1:1	64.70	2.34	0.78	12.76	23.22
US0.5-EH1:1-DP1:1	62.43	2.48	0.63	10.30	21.69
US0.5-EH1:1-TP1:1	57.75	2.32	0.64	22.81	20.10
US0.5-EH1:1-DTP1:1:1	66.02	2.41	0.68	14.91	17.82
US0.5-K1.5-M2.5	65.66	2.35	1.12	15.00	16.36
US0.5-K1.5-T2.5	57.47	2.33	0.79	15.04	26.14
US0.5-K1.5-DT1:1	60.66	2.31	0.76	13.00	24.75

"US ultrasound; EH EDC—HOBt; K KOH; T TEPA; P PEI; D DEA; M MEA; PZ piperazine. The number beside US denotes sonication time in minutes. The number beside EH denotes ratio of activating agents. The number beside K denotes loading of KOH (weight of KOH to the weight of biochar). The number beside T, P, D, M, and PZ denotes amine loading. The numbers beside TD, TP, PD, TM, and TPD denote weight ratio of amines.

3.1.2. BET Analysis. According to the IUPAC, adsorption pores can be classified into three groups: micropore (diameter < 2 nm), mesopore (2 nm < diameter < 50 nm), and macropore (diameter > 50 nm).³³ The values of surface areas as summarized in Table 2 show that the biochar consists of mainly micropores (described by DR-CO₂) with a smaller quantity of mesopores (described by BET-N₂) (312.31 vs 46.93 m²/g, respectively). Under ultrasound irradiation physical effects such as microstreaming, shock waves, and especially microjets result in direct erosion of a particle's surface. ^{19,34} Consequently, the microporous surface area for US0.5-EH0-A0 was enhanced as some new micropores were formed and some blocked pores were opened as observed in Table 2 and Figures 3c.

In this work, micro- and mesoporosities were studied through adsorption of CO_2 and N_2 , respectively. However, it is worth noting that CO_2 can determine only microporous surface areas, while N_2 estimates both micro- and mesoporous surface areas. However, CO_2 and N_2 display certain

differences when measuring microporous surface area since the CO_2 molecule (0.34 nm) is smaller than the N_2 molecule (0.36 nm). Besides, the analysis with CO_2 is conducted at 273 K whereas N2 requires 77 K. Also, at 273 K the saturation pressure of CO_2 is 3.5 MPa, while at 77 K the saturation pressure of N_2 is 0.35 kPa.³⁶ Due to the extremely low saturation pressure, the number of N₂ molecules is significantly lower, and diffusion is also slower than with CO₂. This also lowers the relative pressure range (p/p_0) for CO_2 compared to N_2 (since p_0 for $N_2 \ll p_0$ for CO_2). For these reasons, N_2 only diffuses to the wide micro- and mesopores of the material, but CO₂ diffuses into the narrow micropores. Furthermore, the literature also suggests that the main source of heterogeneity for microporous solids like biochars is their complex porous structure which contains micropores of different dimension and shape such as wider micropores and narrower micropores.³⁷ The biochars used for the present study possess highly heterogeneous microporous structures with different shapes of micropores (wide and narrow). The CO₂-DR analysis

Table 4. Elemental Analysis of Biochars As Percentage of Organic Constituents, Omitting Ash Contribution^a

sample	C content (% wt)	H content (% wt)	N content (% wt)	O content (% wt)	C/N	C/H
raw biochar	83.02	2.50	0.23	14.25	421	5.53
US0.5-EH1:1-M2.5	78.87	2.97	1.43	16.72	64.4	4.42
US0.5-EH1:1-PZ2.5	76.21	3.08	0.50	20.20	178	4.12
US0.5-EH1:1-D2.5	80.37	2.82	0.71	16.11	132	4.75
US0.5-EH1:1-P2.5	78.74	2.86	0.59	17.81	156	4.59
US0.5-EH1:1-MT1:1	76.70	2.95	1.62	18.73	55.2	4.33
US0.5-EH1:1-DT1:1	80.29	2.90	0.97	15.84	96.6	4.61
US0.5-EH1:1-DP1:1	82.31	3.27	0.83	13.58	116	4.19
US0.5-EH1:1-TP1:1	69.14	2.78	0.77	27.31	105	4.14
US0.5-EH1:1-DTP1:1:1	78.58	2.87	0.81	17.75	113	4.56
US0.5-K1.5-M2.5	78.04	2.79	1.33	17.83	68.5	4.66
US0.5-K1.5-T2.5	75.99	3.08	1.04	19.89	85.2	4.11
US0.5-K1.5-DT1:1	79.05	3.01	1.00	16.94	92.2	4.37

"US ultrasound; EH EDC—HOBt; K KOH; T TEPA; P PEI; D DEA; M MEA; PZ piperazine. The number beside US denotes sonication time in minutes. The number beside EH denotes ratio of activating agents. The number beside K denotes loading of KOH (weight of KOH to the weight of biochar). The number beside T, P, D, M, and PZ denotes amine loading. The numbers beside TD, TP, PD, TM, and TPD denote weight ratio of amines.

determines the narrow micropores and the BET- N_2 analysis estimates both wider micropores and mesopores (as tabulated in Table 2). This microporous behavior has been further described in the adsorption isotherm study.

Based on the porous nature of the biochars, the amines can be attached either through impregnation or through grafting. For impregnation, the amine molecules are dispersed inside the pores and over the internal and external surfaces of pores through weak van der Waals force. The grafting, the amine molecules are chemically attached with the surface functional groups through strong covalent bonds. Primarily, the amines are attached to the functional groups and depending on the size, the amine molecules disperse into either of the pores (either micro or macro). Short amines like monoethanolamine preferably enter micropores. However, the highly branched PEI cannot go inside micropores and so requires mesoporous support for attachment. TEPA can also be grafted onto the surface of the porous materials (mesopores) without destroying the intrinsic structure of the sorbent.

Our previous study showed that 30 s of ultrasound irradiation was intense enough to produce maximum microporous surface area and adsorption capacity. Upon further increase of the sonication time, cavitation disarranged the orientation of the layered structure of biochar, consequently blocking the pores and reducing the adsorption capacity. Similar phenomena were observed by Verma et al. and Hamdaoui et al. Furthermore, it is observed from Table 2 that both surface area (based on CO₂ and N₂ analysis) and pore volume of biochar were decreased by amine functionalization, indicating that amines physically loaded on the solid support formed a layer that blocked some of the pores. Similar observations have also been reported by Yue et al. and Teng et al. where they used TEPA-grafted mesoporous silica and KOH-amine modified silica, respectively, for CO₂ adsorption.

3.1.3. Elemental Analysis. The effects of different amine mixtures with EDC-HOBt or KOH activation on the C, H, N, O, and ash content are presented in Table 3. Since the ash content varied widely, pure organic compositions were also calculated by omitting the contribution of ash (Table 4). As can be seen from the Table 3, amination of biochar increased the % N from 2 times to over 7 times its value in raw biochar. TEPA, with 5 amine groups, is very effective in increasing

nitrogen content⁴ since it has 37% N, followed by PZ, MEA, and DEA with 32%, 23%, and 13% N, respectively. Comparing Tables 3 and 4, the observed % N content increments follow the order TEPA-MEA > MEA > TEPA-DEA > TEPA-DEA-PEI > TEPA-PEI > PEI-DEA, with the other singleamine samples lower. Despite its high nitrogen content, PZactivated samples showed only moderately enhanced nitrogenation; since PZ is somewhat volatile, its concentration tends to fall with time. 42 This trend is consistent with the % N of the individual amines as discussed above. For example, a higher value of % N in MEA than DEA resulted in an elevated % N in biochar treated with the binary system TEPA-MEA compared with TEPA-DEA. In the biochar samples activated with DEA-PEI, TEPA-PEI, or DEA-TEPA-PEI, nitrogen attachment was lower than that in MEA-TEPA or DEA-TEPA. This could be due to agglomeration of PEI due to its high molecular weight and polymeric structure that would reduce the other amines' (DEA and TEPA) accessibility to the biochar surface.⁵ Additionally, it was observed comparing Tables 3-4 and 6-7 that the % N content and the adsorption capacity followed the same trend with the maximum adsorption capacity for MEA activated sample that has highest nitrogen content.

Furthermore, the oxygen content of the treated samples was typically somewhat enhanced compared to raw biochar: this indicates the oxygenation of the biochar surface upon activation. During sonication, water undergoes dissociation into $H \bullet$ and $\bullet OH$ radicals.⁴³ Addition of $\bullet OH$ to biochar π bonds would oxidize it, thereby increasing its oxygen content. KOH activation could also enhance oxygenation, for example by saponifying ester groups or opening epoxides.⁴⁴ Air oxidation of the carbon framework is also a possibility.

From Tables 3 and 4, it can be noted that the varying C, N, and H content of the adsorbed amines caused variations in the C/N and C/H molar ratios of the aminated biochars (Table 4). For instance, raw biochar had C/N and C/H ratios of 421 and 5.53, respectively. Modification with MEA, which has lower values of C/N and C/H, significantly decreased the C/N and C/H molar ratios of US0.5-EH1:1-M2.5 to 64.4 and 4.42, respectively. Similar changes were observed for the rest of the amine functionalized samples. Similar explanations were

provided by Zhou et al.⁴⁵ and Yue et al.^{41b} for the variation of elemental compositions of their amine activated adsorbents.

Physicochemical activation of the samples usually led to reduction of the % ash, which is a key factor in increasing the adsorption efficiency and heating value of biochar (Table 4). A decrease in ash content represents the removal of minerals, as well as the enhancement of organic contents, upon activation or amination. The previous studies showed that ultrasound is very useful in leaching the minerals from the structure and making room for amines to attach.⁴ Thus, the reduced ash content helped in incorporation of a greater number of amine groups in the structure, resulting in improved CO₂ adsorption efficiency of the prepared adsorbent. However, few samples showed enhancement of ash content after amination. KOH activation could be a reason for increased ash content (potassium as a mineral add up to the ash) for the samples US0.5-K1.5-T2.5 and US0.5-K1.5-TD1:1. But for US0.5-EH1:1-PZ2.5 activated biochar ash content went up as well which requires further investigation to determine the reason for increased ash content.

3.1.4. Raman Analysis. Raman spectroscopy is a common vibrational spectroscopy technique for investigating the microstructure and mineralogy of carbonaceous compounds such as biochar.²⁷ Raman spectra of raw and singly functionalized biochar with MEA, PZ, DEA, and PEI are shown in Figure 4. Sonication duration, activating agents

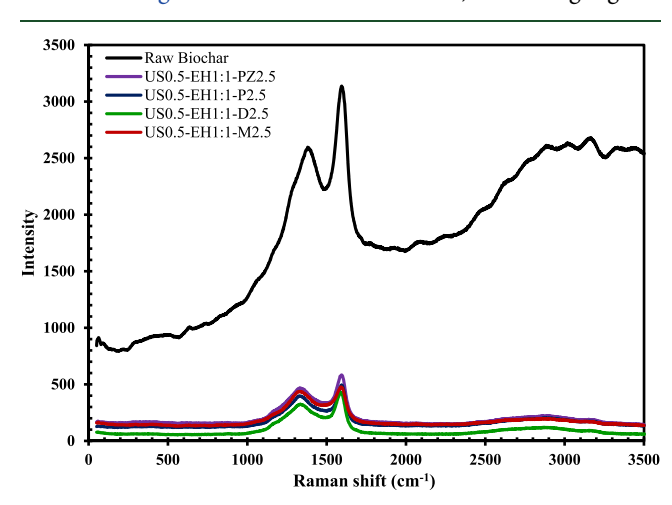


Figure 4. Raman spectra of raw biochar, US0.5-EH1:1-M2.5, US0.5-EH1:1-PZ2.5, US0.5-EH1:1-D2.5, and US0.5-EH1:1-P2.5.

(EDC-HOBt) ratio, and amine concentration for all the samples were maintained at 30 s, 1:1, and 2.5 times weight, respectively. The G band for these spectra appeared at 1591, 1604, 1551, 1592, and 1600 cm⁻¹, and the D band appeared at 1346, 1396, 1336, 1376, and 1359 cm⁻¹ for raw biochar, US0.5-EH1:1-M2.5, US0.5-EH1:1-PZ2.5, US0.5-EH1:1-D2.5, and US0.5-EH1:1-P2.5, respectively. In addition to that, a strong peak (2D) was observed in the range of 2500-2800 cm⁻¹ for the raw biochar sample. These are the signature peaks of graphitic sp² structure that confirm the structural similarity of biochar and graphene oxide. 46 The G-band of the structure is attributed to the vibration of sp² carbon atoms found in graphitic materials, while the D-band is linked to the breathing modes of disordered graphite rings in the form of functionalities such as -OH, -C=O, and -COOH.⁴⁷ The ratio between the intensities of the D and G bands reflects disorder of the biochar structure due to the presence of oxygen

functionalities. ⁴⁸ The values of intensity ratios (I_D/I_G) of raw and activated biochar samples are summarized in Table 5. The

Table 5. Raman Intensity Ratios I_D/I_G of Raw Biochar and Physicochemically Activated Biochars^a

sample name	intensity ratio
raw biochar	0.78
US0.5-EH1:1-M2.5	0.93
US0.5-EH1:1-PZ2.5	0.82
US0.5-EH1:1-D2.5	0.88
US0.5-EH1:1-P2.5	0.87
US0.5-EH1:1-MT1:1	0.95
US0.5-EH1:1-DT1:1	0.80
US0.5-EH1:1-DP1:1	0.85
US0.5-EH1:1-TP1:1	0.86
US0.5-EH1:1-DTP1:1:1	0.93
US0.5-K1.5-T2.5	0.86
US0.5-K1.5-M2.5	0.85
US0.5-K1.5-DT1:1	0.85

"US ultrasound; EH: EDC—HOBt; K KOH; T TEPA; P PEI; D DEA; M MEA; PZ piperazine. The number beside US denotes sonication time in minutes. The number beside EH denotes ratio of activating agents. The number beside K denotes loading of KOH (weight of KOH to the weight of biochar). The number beside T, P, D, M, and PZ denotes amine loading. The numbers beside TD, TP, PD, TM, and TPD denote weight ratio of amines.

activated biochars had higher values of $I_{\rm D}/I_{\rm G}$ than raw biochar, reflecting the enhanced functionalities created by physicochemical modification with sonication and amination. The $I_{\rm D}/I_{\rm G}$ for raw biochar, US0.5-EH1:1-M2.5, US0.5-EH1:1-PZ2.5, US0.5-EH1:1-D2.5, and US0.5-EH1:1-P2.5 were 0.78, 0.93, 0.82, 0.88, and 0.87, respectively. $I_{\rm D}/I_{\rm G}$ was highest for the MEA-modified sample, followed by DEA, PEI, and PZ for the single amine systems. The elemental analysis and the CO₂ adsorption results followed the same trend: elemental analysis (Table 3) showed the nitrogen content in MEA, DEA, PEI, and PZ-modified samples was 8, 3, 2.6, and 2 times higher than that in raw biochar, respectively. Correspondingly, the adsorption capacity was maximum for US0.5-EH1:1-M2.5 (Table 6), compared to other amine activated samples.

In Figure 5, the Raman spectra of binary and ternary amine mixtures are reported. Sonication duration and activating agent ratio (EDC–HOBt) for all the samples were maintained at 30 s and 1:1, respectively. The intensity ratio $I_{\rm D}/I_{\rm G}$ had the following values: 0.95, 0.80, 0.85, 0.86, and 0.93 for US0.5-EH1:1-MT1:1, US0.5-EH1:1-DT1:1, US0.5-EH1:1-DP1:1, US0.5-EH1:1-TP1:1, and US0.5-EH1:1-DTP1:1:1, respectively. The maximum departure of the $I_{\rm D}/I_{\rm G}$ ratio was found for US0.5-EH1:1-MT1:1, suggesting that the maximum defects resulted from amination by the binary MEA–TEPA mixture. This is in accordance with the CO₂ sorption result (Table 6), showing that dual amination with MEA and TEPA using EDC–HOBt as activating agents provided a favorable combination for achieving improved adsorption capacity.

Finally, the Raman spectra of KOH-activated amine functionalized samples are presented in Figure 6. The figure shows that the G peaks are located at 1615, 1602, and 1592 cm⁻¹ and the D peaks are located at 1404, 1342, and 1331 cm⁻¹ for US0.5-K1.5-M2.5, US0.5-K1.5-T2.5, and US0.5-K1.5-DT1:1, respectively. The increased values of the intensity ratios (0.85, 0.86, 0.85 respectively, from Table 5) compared

Table 6. CO₂ Adsorption Capacities (mmol/g) of Biochars (Raw and Functionalized) at 70 °C and 10 vol % CO₂ (Effects of EDC-HOBt-activated Amines and Amine Mixtures)^a

sample	amine	amine	loading (times 1	mass of biochar)		CO ₂ conc (vol %)
		2.5	5	10	0	
			adsorption ca	apacity		
raw biochar	none				0.30	10
US3-EH0-T0	none				0.55	10
US0-EH1:1-T2.5	TEPA	0.56				10
US0.5-EH1:1-M2.5 ^b	MEA	1.74 ± 0.04	1.81	1.84		10
US0.5-EH1:1-PZ2.5	PZ	1.02	1.12	1.13		10
US0.5-EH1:1-D2.5 ^b	DEA	1.05 ± 0.05	1.14	1.16		10
US0.5-EH1:1-T2.5	TEPA	2.044				10
US0.5-EH1:1-P2.5 ^b	PEI	1.02 ± 0.08	1.12	1.13		10
US0.5-EH1:1-MT1:1 ^b	MEA-TEPA	1.91 ± 0.02				10
US0.5-EH1:1-DT1:1	DEA-TEPA	1.45				10
US0.5-EH1:1-DP1:1	DEA-PEI	1.08				10
US0.5-EH1:1-TP1:1	TEPA-PEI	1.20				10
US0.5-EH1:1-DTP1:1:1 ^b	DEA-TEPA-PEI	1.20 ± 0.04				10
US0.5-EH1:1-T2.5	TEPA	2.93				100
US0.5-EH1:1-MT1:1	TEPA	2.21				100

"US ultrasound; EH EDC-HOBt; M MEA; PZ piperazine; D DEA; T TEPA; P PEI. Number beside US denotes sonication time in minutes; 1:1 beside EH denotes an equal ratio of activating agents; 2.5 beside M, PZ, D, T, P denotes amine loading; 1:1 beside MT, DT, DP, TP and DTP denotes an equal weight ratio of amines to biochar. "Values are averages of duplicate runs ± standard deviation."

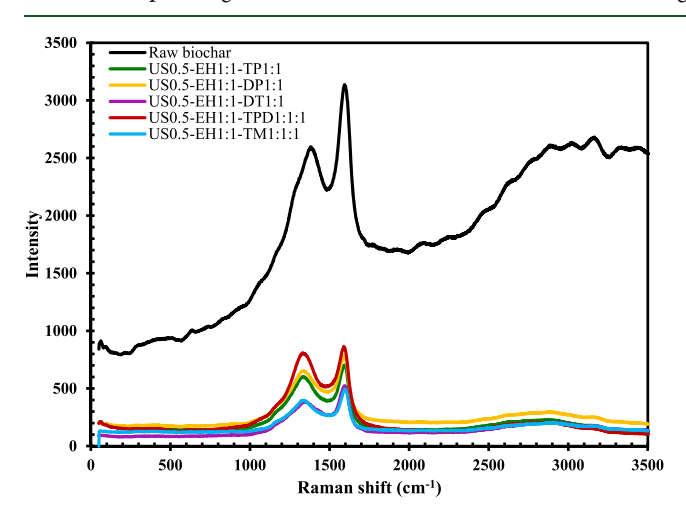


Figure 5. Raman spectra of raw biochar, US0.5-EH1:1-MT1:1, US0.5-EH1:1-DT1:1, US0.5-EH1:1-DT1:1, US0.5-EH1:1-TP1:1, and US0.5-EH1:1-DTP1:1:1.

to raw biochar are indicators of higher quantity of defects (functional groups) on the sorbents' surfaces due to activation. This is consistent with the changes in adsorption capacity (Table 7). The elemental analysis results showed that the maximum gain in nitrogen content among the KOH-aminated samples was obtained for US0.5-K1.5-M2.5, slightly less than the N gain for EDC—HOBt activation (US0.5-EH1:1-M2.5). Therefore, the biochar samples treated with KOH (as activating agent) and subsequently functionalized with amine (MEA) could be an alternative to the EDC—HOBt—amine functionalization technique. Nonetheless, this needs further thorough study for intensifying and optimizing the results.

3.1.5. FTIR Analysis. The IR spectra of the biochar samples functionalized with EDC-HOBt and amines individually and their binary-ternary mixtures are shown in Figures 7 and 8, respectively. The FTIR bands for the samples activated with

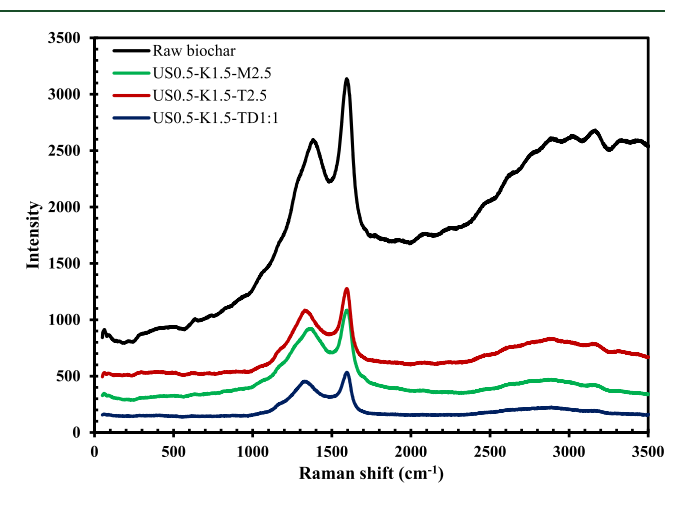


Figure 6. Raman spectra of raw biochar, US0.5-K1.5-M2.5, US0.5-K1.5-T2.5, and US0.5-K1.5-DT1:1.

KOH and amines (single: MEA, TEPA, and binary: DEA-TEPA) are represented in Figure 9. The FTIR spectra had similar shapes for both raw and functionalized biochars. However, due to functionalization, some new peaks were generated. For instance, a new peak at 870 cm⁻¹ was observed for all the activated samples that is attributed to the out of plane bending of N-H groups formed due to primary and secondary amines. 50 The band is most significant for the sample US0.5-EH1:1-M2.5 (Figure 7), demonstrating that MEA is more effective in grafting amino groups than the other amines. At \sim 1430 cm $^{-1}$ a peak was observed for the same sample US0.5-EH1:1-M2.5 (Figure 7), which could be attributed to C–H bending from sp³ carbons, representing the methylene groups that are part of MEA. A peak in the region of 3300-3500 cm⁻¹ was observed due to -OH (and -NH) stretching vibration and existed in all biochar samples.⁴ For KOH activated samples, shown in Figure 9, the band at 1097 cm⁻¹ was intense, representing a high degree of

Table 7. Effect of KOH-Amine Mixture on CO₂ Adsorption Capacity at 70 °C and 10 vol % CO₂ Concentration^a

sample name	adsorption capacity (mmol/g)	CO ₂ concentration (vol %)
Raw Biochar	0.3	10
US0.5-K1.5-M2.5	1.62	10
US0.5-K1.5-P2.5	1.00	10
US0.5-K1.5-D2.5	1.08	10
US0.5-K1.5-T2.5 ^b	1.60 ± 0.05	10
US0.5-K1.5-DT1:1	1.38	10
US0.5-K1.5-TP1:1	1.12	10
US0.5-K1.5-M2.5	1.93	100
US0.5-K1.5-DT1:1	1.79	100

^aUS ultrasound; K KOH; T TEPA; P PEI; D DEA; M MEA. The number beside US denotes sonication time in minutes. The number beside K denotes loading of KOH (weight of KOH to the weight of biochar). The number beside T, P, D, and M denotes amine loading. The numbers beside TD and TP denote weight ratio of amines. ^bValue is the average of duplicate runs \pm standard deviation.

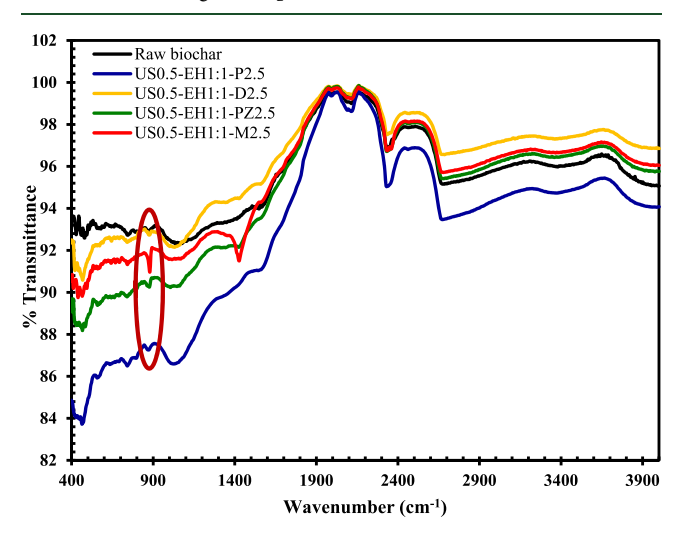


Figure 7. FTIR spectra of raw biochar, US0.5-EH1:1-M2.5, US0.5-EH1:1-PZ2.5, US0.5-EH1:1-D2.5, and US0.5-EH1:1-P2.5.

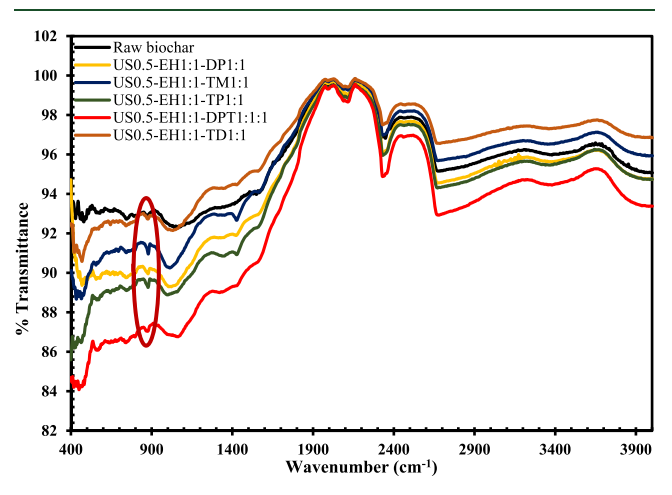


Figure 8. FTIR spectra of raw biochar, US0.5-EH1:1-MT1:1, US0.5-EH1:1-DT1:1, US0.5-EH1:1-DT1:1, EH1:1-TP1:1, and US0.5-EH1:1-DTP1:1:1.

oxygenation due to formation of C-O bonds. A more distinct carbonyl peak was observed for the KOH-amine activated

I

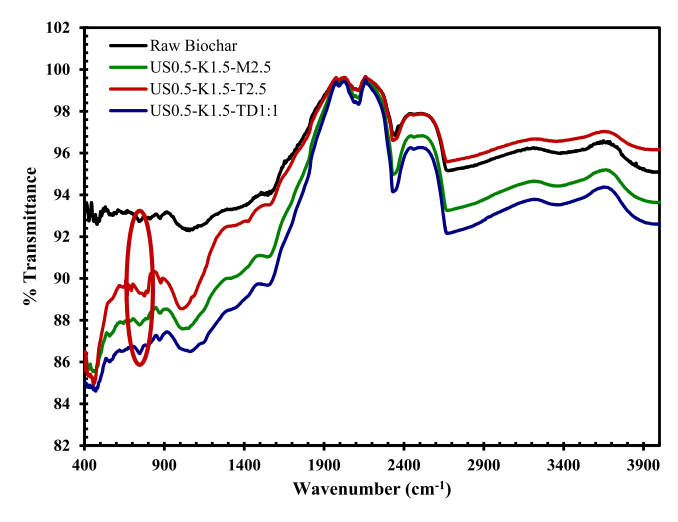


Figure 9. FTIR spectra of raw biochar, US0.5-K1:5-M2.5, US0.5-K1:5-T2.5, and US0.5-K1:5-DT1:1.

samples at 1600 cm⁻¹ in Figure 9, which could reflect additional carboxyl groups following saponification.

3.2. CO₂ Adsorption Studies. 3.2.1. CO₂ Adsorption with Amine Systems Activated by EDC–HOBt. The CO₂ adsorption capacities of biochar samples aminated with individual, binary, and ternary combinations of MEA, PZ, DEA, TEPA, and PEI are summarized in Table 6. The effect of TEPA alone was studied in our previous work⁴ and is included in the table for reference.

Besides, two control tests were separately conducted which showed the effect of individual activation processes on CO₂ adsorption (see Table 6). In one test, a biochar sample was chemically activated with TEPA (no ultrasonic irradiation), while the focus of the other test was only on physical activation under ultrasound irradiation (no TEPA). Comparison of the results of the two control tests with the integrated physicochemical activation exhibited the following adsorption range: physicochemical activation (2.04 mmol/g) \gg chemical activation (0.56 mmol/g) ~ physical activation (0.55 mmol/ g). The result showed that the samples activated with either ultrasound or amine individually possess very limited adsorption capacity, while integrated activation strategies have had a significant effect on the CO₂ adsorption of biochar. This further demonstrates the effectiveness of the combined physical and chemical activation technique.

To study the effect of amine concentrations on CO₂ removal the amine loading was varied from 2.5 to 10 times the weight of the biochar. The results showed an increasing trend in adsorption capacity with amine loading. However, the increase in adsorption capacity was small after the initial increase of amine loading. Higher concentrations of impregnating amines during activation can supply more active sites but can also block the pores and result in lower adsorption values. This is in accordance to our previous research that demonstrated TEPAactivated biochar showed a maximal adsorption capacity (7 times higher than raw char) for CO₂ (2.04 mmol/g) with an optimal 2.5 times loading. Therefore, in this study, sorbents were prepared with MEA, PZ, DEA, TEPA, and PEI at the same 2.5 times total amine loading to investigate their effects on CO2 adsorption capacity. The amine mixtures were set at a total 2.5 times loading to the weight of the biochar, with equal weight of the individual amines in the mixture.

Table 8. Comparison of Adsorption Capacity Obtained in Present Study with Literature Work

support material	amine	adsorption capacity	ref
mesoporous silica	TEPA	3.93	40
MCM-41	TEPA	5.39	65
nanofibrillated cellulose	N-(2-aminoethyl) 3-aminopropylmethyldimethoxysilane	1.39	55
saw dust biochar	MEA	1.02	66
aminated graphene oxide	EDA, DETA, TETA	1.10	67
palm shell activated carbon	DEA	2.81	68
SBA-15	PEI	2.39	69
nanocomposite sorbent	PEI	7.90	51
mesoporous carbon	PEI-KOH	4.82	70
pine wood biochar	TEPA	2.04	4
SBA-12 mesoporous silica	3-aminopropyl (AP)	1.04	56
cotton stalk	ammonia and CO ₂	2.25	71
sawmill residues	aminopropyl triethoxysilane	3.70	72
fly carbon	DETA, PEHA, PEI	1.56	57
pine wood biochar	TEPA	2.04	4
pine wood biochar	TEPA-MEA	1.91	this study
pine wood biochar	MEA-KOH	1.61	this study

Among the single amines, it can be observed from Table 6 that TEPA provided the maximum adsorption capacity (2.04 mmol/g), with MEA (1.74 mmol/g) notably stronger than the others. TEPA is aided by the five amino groups in its structure and by its less viscous nature compared to PEI. Among the blended mixtures, MEA—TEPA-activated biochar provided the maximum adsorption capacity (1.91 mmol/g), followed by DEA—TEPA, DEA—TEPA—PEI, TEPA—PEI, and DEA—PEI.

Furthermore, the combinations MEA–TEPA and DEA–TEPA were aided by the presence of the hydroxyl groups in MEA and DEA. For example, hydroxyl groups are known to enhance CO_2 adsorption capacity on silica substrates as adsorbents. To explain this effect, consider that the acid–base reaction of amines with carbonic acid $O=C(OH)_2$, formed by the addition of H_2O to CO_2 , can sequester CO_2 in the form of either hydrogen carbonate or carbonate anions:

$$RNH_2 + CO_2 + H_2O \rightarrow RHN_3^+ + HCHO_3^-$$

 $2RNH_2 + CO_2 + H_2O \rightarrow 2RHN_3^+ + CO_3^{2-}$

Alternatively, an amine can attack CO₂ covalently to form a carbamate anion, also balanced by an ammonium cation:

$$2RNH_2 + CO_2 \rightarrow RNH_3^+ + RNH - CO_3^-$$

A possible role of alcohols in promoting these reactions is in offering hydrogen bonding to stabilize the anionic product oxygens; O-H is a better hydrogen bond donor than N-H, so alcohols can perform this role better than amines. Another suggestion is that the alcohols aid in making the amine chains more flexible, making it easier for them to carry out the proton transfers required to attain the ionic products.⁵² PZ may be hindered by the absence of hydroxyl groups as well as the lack of a 1° amine. Note that the balance of amino and hydroxyl groups matters: DEA had a low capacity in spite of two hydroxyls, since it has only a single 2° amine. The mixture of TEPA-PEI, without hydroxyl groups, had an adsorption capacity notably lower than the DEA-TEPA and MEA-TEPA mixtures. Another factor that affects sorption capacity is the low diffusion ability of the large PEI molecules, which could hinder their ability to effect proton transfers. Also, the more viscous PEI (compared to the other amines) tends to form agglomerations on the surface of the sorbent, thus reducing active sites for adsorption (observed from Table 2). All of the PEI samples had low adsorption capacities.

Several of the runs were performed in duplicate, and their standard deviations are included in Table 6. Standard deviations were in the range of 0.02–0.08, showing that the differences in adsorption capacity observed are significant.

3.2.2. CO₂ Adsorption with Amine Systems Activated by KOH. The adsorption capacities of KOH-amine activated samples are listed in Table 7. As shown in Table 3 (elemental analysis), pretreatment of biochar with KOH increased the % N in samples impregnated with amines, similar to the increase noted with EDC-HOBt activation. The CO₂ adsorption capacities were also much greater than that for raw biochar, although somewhat lower than for samples aminated with EDC-HOBt. This could be attributed to the destruction of some surface structure porosity due to application of the powerful base. This is also reflected in the surface area analysis (Table 2) where the surface area and pore volume were reduced for KOH-aminated samples.

There remains the question of the extent of activation of KOH toward amination of the sonicated biochar. There is a report that solid NaOH can catalyze the alkylation of amines with alcohols via a hydride transfer from the corresponding alkoxide, forming an intermediate aldehyde.⁵³ However, this process requires high temperatures (>180 °C). It has also been reported that carbonyl groups in carbonaceous material are able to catalyze the same reaction through a "borrowing hydrogen" mechanism. 54 However, this process also requires a high temperature (>130°). It may be that, through saponification of esters or alteration of the pore structure, the KOH provides more sites for hydrogen bonding of the impregnated amines and hydroxyamines with the biochar surface. Regardless, due to its simplicity, this technique may have wide application in sorbent synthesis. However, it will require further research and analysis to establish this procedure as a useful CO₂ capture technique.

Furthermore, as observed from the CO_2 adsorption result the adsorption capacity of the amine functionalized sorbent was enhanced in comparison with the pristine biochar at 70 $^{\circ}$ C. This can be explained based on the differences of physical adsorption or physisorption, and chemical adsorption or chemisorption. Usually, physisorption is dominant at room

temperature over chemisorption. However, at elevated temperatures, chemisorption is more dominant than physisorption as a result of amine functionalization. Thus, even though the surface area and pore size reduced due to amine attachment, still improved capacity was attained at higher temperature, due to increase in the chemisorption process. The details discussion can be found in our previous study.⁴

Additionally, in order to confirm the effectiveness of the developed activation technique, the adsorption capacity of the prepared adsorbent (present study) has been compared with the literature data as shown in Table 8. It can be concluded from the table that the ultrasono-amine functionalized adsorbent material has comparatively higher adsorption capacity (2.04 mmol/g) than several adsorbents such as biochars, activated carbon, graphene oxide, and SBA-12.55-57 However, the adsorption capacity of aminated biochar did not reach the optimum or maximum level as found for ordered mesoporous silica functionalized with amines. This can be explained as a result of blocking the pores (primarily micropores) of carbon structure due to the introduction of nitrogen or other chemical functionalities.⁵⁸ This subsequently lowers the adsorption capacity. Whereas, for ordered mesoporous materials, because of ordered mesoporous structure with tunable pores, amines or other molecules can be easily accommodated without blocking the surface of the adsorbent owing to their higher adsorption capacity compared to microporous adsorbents.

4. BREAKTHROUGH STUDY OF THE ACTIVATED ADSORBENTS

The dynamic CO₂ adsorption was assessed based on a breakthrough study of adsorption. Figure 10 represents

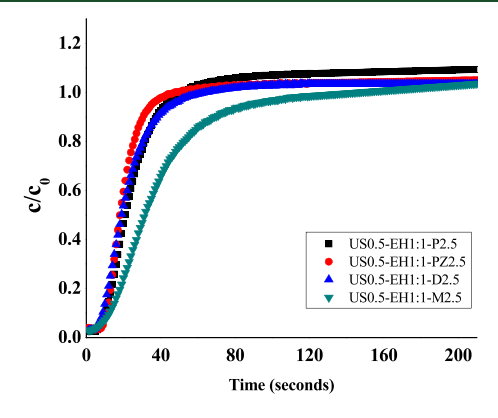


Figure 10. Breakthrough curves for US0.5-EH1:1-M2.5, US0.5-EH1:1-PZ2.5, US0.5-EH1:1-D2.5, and US0.5-EH1:1-P2.5.

different breakthrough plots for single amine systems (out of 30 min). As observed, all the curves show a similar trend. However, the steeper the curve, the higher will be the mass transfer resistance. Therefore, among all the samples in Figure 10, US0.5-EH1:1-M2.5 has the minimum resistance and subsequently the maximum capacity. This is consistent with the amine size. Since the MEA molecule is small, it will exert less resistance and provide a higher mass transfer rate and improved capacity. Highly polymeric PEI and viscous DEA impart high mass transfer resistance and less adsorption efficiency compared to MEA. PZ has limited solvent solubility, resulting in subsequent precipitation and low CO₂ removal. Figure 11 represents the breakthrough curves of the blended

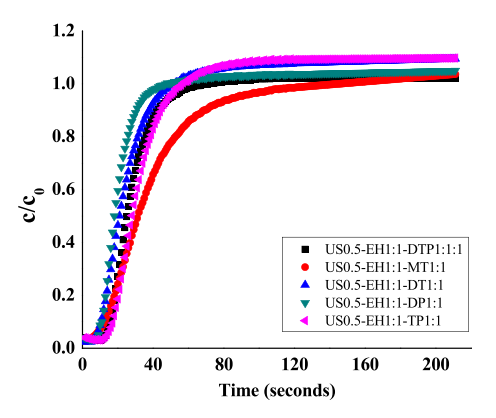


Figure 11. Breakthrough curves for US0.5-EH1:1-DP1:1, US0.5-EH1:1-DT1:1, US0.5-EH1:1-MT1:1, US0.5-EH1:1-TP1:1, and US0.5-EH1:1-DTP1:1:1.

amine systems. As per the breakthrough analysis, US0.5-EH1:1-MT1:1 exhibits the least steep curve among other blended sorbent materials that corresponds to the maximum sorption ability. This is attributed to the high reactivity and sorption capacity of MEA modified by the reduced sorption capacity of TEPA due to the influence of the alkyl group present in its structure. Therefore, the use of blended solution of MEA and TEPA is a useful technique to enhance sorption characteristics. In accordance to the previous discussion for single amine system, the other amine mixtures such as TEPA-PEI, DEA-PEI, DEA-TEPA, and DEA-TEPA-PEI exhibit low adsorption efficiency as a result of decreased mass transfer rate, viscous nature, and low solvent volatility. The breakthrough curve in Figure 12 depicts the

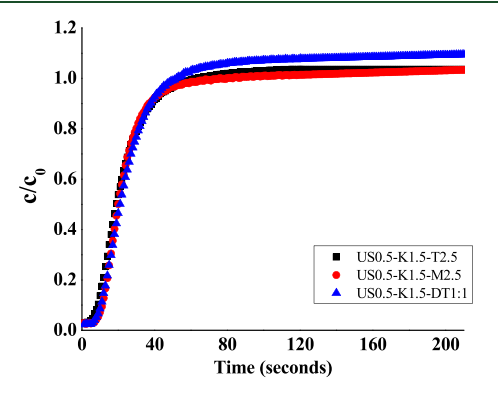


Figure 12. Breakthrough curves for US0.5-K1.5-M2.5, US0.5-K1.5-T2.5, and US0.5-K1.5-DT1:1.

behavior of the biochar system activated with KOH and amines. The sample activated with KOH–MEA exhibits maximum adsorption efficiency compared to the other KOH–amine activated samples as a result of improved mass transfer efficiency of the MEA molecule with respect to the other amines, which is in accordance to the previous explanation.

Additionally, and in order to investigate the maximum adsorption capacity of the activated biochars, four extra adsorption tests were conducted under pure CO₂. The samples included ultrasono-activated biochar followed by (i) EDC–HOBt–TEPA; (ii) EDC–HOBt–MEA–TEPA; (iii) KOH–MEA; and (iv) KOH–DEA–TEPA. These samples have shown the maximum adsorption capacity under 10 vol % of

CO₂. The breakthrough curve is plotted in Figure 13 with their adsorption capacity data in Tables 6–7. As expected, the

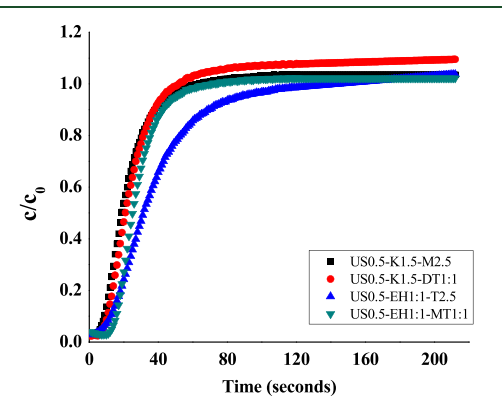


Figure 13. Adsorption breakthrough curves of US0.5-EH1:1-T2.5, US0.5-EH1:1-MT1:1, US0.5-K1.5-M2.5, and US0.5-K1.5-DT1:1 (under a pure CO₂ environment)

adsorption capacities for the samples under pure $\rm CO_2$ environment are significantly higher compared to the previously tested samples. This attributes to the presence of higher number of $\rm CO_2$ molecules and increased interaction between adsorbate and adsorbent that resulted in the enhanced adsorption capacity. However, the desired operating condition for dynamic adsorption tests are under simulated flue gas conditions consisting of $10{-}15$ vol % of $\rm CO_2$ which was the focus of our study.

5. ADSORPTION ISOTHERMS FOR ACTIVATED ADSORBENTS

The CO_2 adsorption isotherms of the samples were obtained at low temperature (273 K). The isotherms are the indicator of the adsorptive capacity of the adsorbents. Figure 14 represents

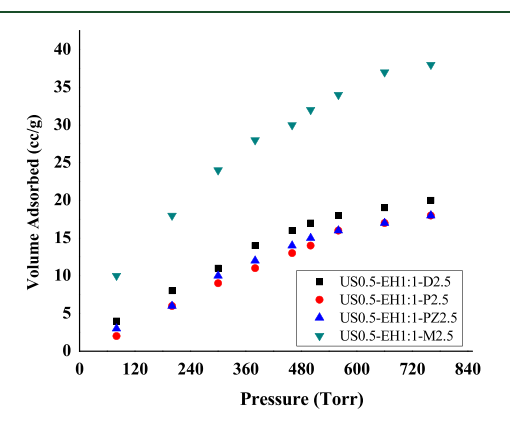


Figure 14. CO₂ adsorption isotherms of US0.5-EH1:1-M2.5, US0.5-EH1:1-PZ2.5, US0.5-EH1:1-D2.5, and US0.5-EH1:1-P2.5.

the isotherms of biochar samples activated with ultrasound and different amines (single amines). The isotherm plots correlate the amount (volume) of gas adsorbed by the adsorbent with respect to the pressure. The higher the adsorbed volume, the better will be the adsorption capacity. As observed from Figure 14, the MEA activated sample has the highest value for adsorbed volume, signifying that this sample has the maximum sorption capacity. This has been further proved based on the equilibrium adsorption capacity presented in Table 6 and surface area analysis (Table 2). Likewise, all the other

isotherms (Figures 14–16) are similar with respect to the equilibrium adsorption capacity (Tables 6–7) and surface area

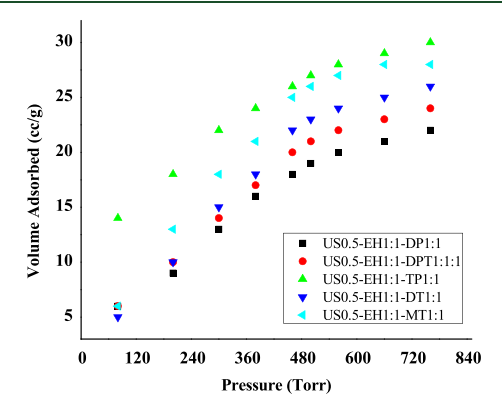


Figure 15. CO_2 adsorption isotherms of US0.5-EH1:1-DP1:1, US0.5-EH1:1-DT1:1, US0.5-EH1:1-MT1:1, US0.5-EH1:1-TP1:1, and US0.5-EH1:1-DTP1:1:1.

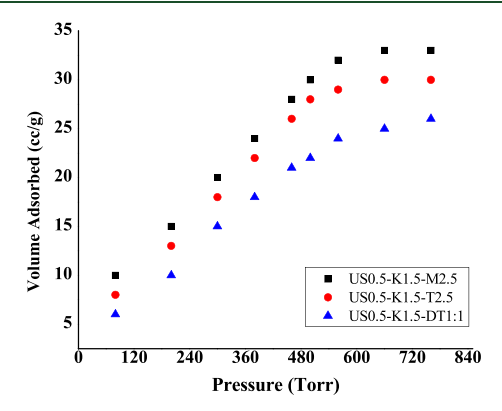


Figure 16. $\rm CO_2$ adsorption isotherms of US0.5-K1.5-M2.5, US0.5-K1.5-T2.5, and US0.5-K1.5-DT1:1.

analysis (Table 2). The curves show that very little adsorption takes place at low pressure, owing to the small interaction force between adsorbate—adsorbent. The capacity enhanced gradually with pressure. Furthermore, the shape of the isotherms is very significant to determine the interaction behavior between adsorbate and adsorbent. The above-mentioned isotherms depict Type I as per IUPAC classification. Type I isotherms are common for microporous solids. When the attractive forces between adsorbed gas and adsorbent are greater than those between the molecules of the gas, it exhibits a Type I isotherm. Thus, the isotherms provide a further confirmation of the adsorption behavior of the prepared adsorbents under different conditions and portray the effectiveness of the developed sono-chemical activation route for enhanced $\rm CO_2$ adsorption.

6. CONCLUSIONS

The current study provides an analysis of the CO_2 adsorption potentials of biochar aminated with five different amines (MEA, PZ, DEA, TEPA, and PEI) and their binary (MEA–TEPA, DEA–TEPA, DEA–PEI, TEPA–PEI) and ternary (DEA–TEPA–PEI) mixtures coupled with ultrasonication and EDC–HOBt or (in 3 cases) KOH activation. Our previous study revealed that physical activation under ultrasound irradiation followed by chemical functionalization with TEPA leads to an elevated adsorption capacity (2.04 mmol/g

at 0.10 atm and 70 °C) compared to raw biochar (0.3 mmol/g at 0.10 atm and 70 °C). This study investigates the effects of different amines that vary in the number of amine groups in their structure. The results showed that primary amine MEA with EDC-HOBt provided the highest adsorption capacity (1.74 mmol/g) after that of TEPA. This is partly attributed to increased reaction rates for 1° amines such as MEA over 2° amines like PZ and DEA.⁶⁴ Functionalization with the MEA-TEPA mixture (with EDC-HOBt) led to 1.91 mmol/g of equilibrium sorption capacity. This indicated the synergetic effect between the hydroxyl in MEA and the amino groups present in TEPA to intensify CO2 capture. For KOH activation, MEA-functionalized sorbent showed the highest equilibrium adsorption capacity of 1.62 mmol/g (5 times higher than raw char). However, the reaction with strong base resulted in the destruction of the surface structure for functionalized sorbents, so the resulting char possessed lower sorption ability than EDC-HOBt-amine modified sorbents. Apart from the promising adsorption results, the sonochemical technique is also very energy efficient since it is done at near room temperature. Hence, the developed ultrasono-amine functionalization technique provided a useful way for efficient functionalization of biochar to produce potential sorbents for CO₂ adsorption.

AUTHOR INFORMATION

Corresponding Author

*E-mail: bsajjadi@olemiss.edu. Tel. No.: 662-915-1640. Fax No.: 662-915-7023.

ORCID ®

Baharak Sajjadi: 0000-0001-6609-0705 Nathan Hammer: 0000-0002-6221-2709

Notes

The authors declare no competing financial interest.

¹Formerly with Chemical Engineering Department, School of Engineering, University of Mississippi, 134 Anderson Hall, Oxford, MS 38677-1848, U.S.A.

ACKNOWLEDGMENTS

The authors are grateful for the financial support of the National Science Foundation (NSF EPSCoR RII Grant No. OIA-1632899 and MRI Grant No. CHE-1532079). Various other supports from the University of Mississippi are also gratefully acknowledged. Also, the authors would like to acknowledge Mr. Cameron Smith (Undergraduate student from the Department of Chemistry and Biochemistry of University of Mississippi) for helping in accomplishing the Raman analysis.

■ REFERENCES

- (1) Levêque, J.-M.; Duclaux, L.; Rouzaud, J.-N.; Reinert, L.; Komatsu, N.; Desforges, A.; Afreen, S.; Sivakumar, M.; Kimura, T. Ultrasonic treatment of glassy carbon for nanoparticle preparation. *Ultrason. Sonochem.* **2017**, *35*, 615–622.
- (2) Dong, Y.; Wang, R.; Li, H.; Shao, J.; Chi, Y.; Lin, X.; Chen, G. Polyamine-functionalized carbon quantum dots for chemical sensing. *Carbon* **2012**, *50* (8), 2810–2815.
- (3) Slowing, I. I.; Trewyn, B. G.; Giri, S.; Lin, V. Y. Mesoporous silica nanoparticles for drug delivery and biosensing applications. *Adv. Funct. Mater.* **2007**, *17* (8), 1225–1236.
- (4) Chatterjee, R.; Sajjadi, B.; Mattern, D. L.; Chen, W.-Y.; Zubatiuk, T.; Leszczynska, D.; Leszczynski, J.; Egiebor, N. O.; Hammer, N. Ultrasound cavitation intensified amine functionalization: A feasible

strategy for enhancing CO₂ capture capacity of biochar. Fuel 2018, 225, 287-298.

- (5) Yu, C.-H.; Huang, C.-H.; Tan, C.-S. A review of CO_2 capture by absorption and adsorption. *Aerosol Air Qual. Res.* **2012**, 12 (5), 745–769
- (6) Samanta, A.; Zhao, A.; Shimizu, G. K.; Sarkar, P.; Gupta, R. Post-combustion CO₂ capture using solid sorbents: a review. *Ind. Eng. Chem. Res.* **2012**, *51* (4), 1438–1463.
- (7) Dillon, D.; Panesar, R.; Wall, R.; Allam, R.; White, V.; Gibbins, J.; Haines, M. Oxy-combustion processes for CO₂ capture from advanced supercritical PF and NGCC power plant. 7th International Conference on Greenhouse Gas Technologies, Vancouver, Canada, 2004.
- (8) Raganati, F.; Ammendola, P.; Chirone, R. On improving the CO₂ recovery efficiency of a conventional TSA process in a sound assisted fluidized bed by separating heating and purging. *Sep. Purif. Technol.* **2016**, *167*, 24–31.
- (9) Riboldi, L.; Bolland, O. Evaluating Pressure Swing Adsorption as a CO₂ separation technique in coal-fired power plants. *Int. J. Greenhouse Gas Control* **2015**, 39, 1–16.
- (10) Plaza, M. G.; García, S.; Rubiera, F.; Pis, J.; Pevida, C. Post-combustion CO₂ capture with a commercial activated carbon: comparison of different regeneration strategies. *Chem. Eng. J.* **2010**, *163* (1–2), 41–47.
- (11) Li, G.; Xiao, P.; Webley, P.; Zhang, J.; Singh, R.; Marshall, M. Capture of CO₂ from high humidity flue gas by vacuum swing adsorption with zeolite 13X. *Adsorption* **2008**, *14* (2–3), 415–422.
- (12) Mason, J. A.; Sumida, K.; Herm, Z. R.; Krishna, R.; Long, J. R. Evaluating metal—organic frameworks for post-combustion carbon dioxide capture via temperature swing adsorption. *Energy Environ. Sci.* **2011**, *4* (8), 3030–3040.
- (13) Laheäär, A.; Delpeux-Ouldriane, S.; Lust, E.; Béguin, F. Ammonia treatment of activated carbon powders for supercapacitor electrode application. *J. Electrochem. Soc.* **2014**, *161* (4), A568–A575.
- (14) Przepiórski, J.; Skrodzewicz, M.; Morawski, A. High temperature ammonia treatment of activated carbon for enhancement of CO₂ adsorption. *Appl. Surf. Sci.* **2004**, 225 (1–4), 235–242.
- (15) Shafeeyan, M. S.; Houshmand, A.; Arami Niya, A.; Razaghizadeh, H.; Daud, W. M. A. W. Modification of activated carbon using nitration followed by reduction for carbon dioxide capture. *Bull. Kor. Chem. Soc.* **2015**, *36* (2), 533–538.
- (16) Al-Warhi, T. I.; Al-Hazimi, H. M.; El-Faham, A. Recent development in peptide coupling reagents. *J. Saudi Chem. Soc.* **2012**, 16 (2), 97–116.
- (17) Lalhruaitluanga, H.; Jayaram, K.; Prasad, M.; Kumar, K. Lead (II) adsorption from aqueous solutions by raw and activated charcoals of Melocanna baccifera Roxburgh (bamboo)—a comparative study. *J. Hazard. Mater.* **2010**, *175* (1–3), 311–318.
- (18) Regmi, P.; Moscoso, J. L. G.; Kumar, S.; Cao, X.; Mao, J.; Schafran, G. Removal of copper and cadmium from aqueous solution using switchgrass biochar produced via hydrothermal carbonization process. *J. Environ. Manage.* **2012**, *109*, 61–69.
- (19) Wu, T. Y.; Guo, N.; Teh, C. Y.; Hay, J. X. W. Advances in ultrasound technology for environmental remediation; Springer Science & Business Media: 2012.
- (20) Zhu, D.; Fang, M.; Lv, Z.; Wang, Z.; Luo, Z. Selection of blended solvents for CO₂ absorption from coal-fired flue gas. Part 1: Monoethanolamine (MEA)-based solvents. *Energy Fuels* **2012**, *26* (1), 147–153.
- (21) Chen, W. Y.; Mattern, D. L.; Okinedo, E.; Senter, J. C.; Mattei, A. A.; Redwine, C. W. Photochemical and acoustic interactions of biochar with CO₂ and H₂O: applications in power generation and CO₂ capture. *AIChE J.* **2014**, *60* (3), 1054–1065.
- (22) Navarro, N. M.; Chave, T.; Pochon, P.; Bisel, I.; Nikitenko, S. I. Effect of ultrasonic frequency on the mechanism of formic acid sonolysis. *J. Phys. Chem. B* **2011**, *115* (9), 2024–2029.
- (23) Ganz, S.; Gutierrez, E. Cavitation: Causes, Effects, Mitigation and Application; Rensselaer Polytechnic Institute: Hartford, CT, USA, 2012.

(24) Qin, J.; Wang, T.-Y.; Willmann, J. K., Sonoporation: applications for cancer therapy. In *Therapeutic Ultrasound*; Springer, 2016; pp 263–291.

- (25) Verma, Y. L.; Singh, M. P.; Singh, R. K. Effect of ultrasonic irradiation on preparation and properties of ionogels. *J. Nanomater.* **2012**, *2012*, 1.
- (26) Hamdaoui, O.; Naffrechoux, E.; Tifouti, L.; Pétrier, C. Effects of ultrasound on adsorption—desorption of p-chlorophenol on granular activated carbon. *Ultrason. Sonochem.* **2003**, *10* (2), 109—114.
- (27) Zhao, L.; Cao, X.; Mašek, O.; Zimmerman, A. Heterogeneity of biochar properties as a function of feedstock sources and production temperatures. *J. Hazard. Mater.* **2013**, *256*, 1–9.
- (28) Heydari-Gorji, A.; Belmabkhout, Y.; Sayari, A. Polyethylenimine-impregnated mesoporous silica: effect of amine loading and surface alkyl chains on CO2 adsorption. *Langmuir* **2011**, 27 (20), 12411–12416.
- (29) Jadhav, P.; Chatti, R.; Biniwale, R.; Labhsetwar, N.; Devotta, S.; Rayalu, S. Monoethanol amine modified zeolite 13X for CO₂ adsorption at different temperatures. *Energy Fuels* **2007**, 21 (6), 3555–3559.
- (30) Mukherjee, A.; Lal, R. Biochar impacts on soil physical properties and greenhouse gas emissions. *Agronomy* **2013**, 3 (2), 313–339.
- (31) Stankovich, S.; Dikin, D. A.; Dommett, G. H.; Kohlhaas, K. M.; Zimney, E. J.; Stach, E. A.; Piner, R. D.; Nguyen, S. T.; Ruoff, R. S. Graphene-based composite materials. *Nature* **2006**, *442* (7100), 282.
- (32) Ohs, B.; Krödel, M.; Wessling, M. Adsorption of carbon dioxide on solid amine-functionalized sorbents: A dual kinetic model. *Sep. Purif. Technol.* **2018**, *204*, 13–20.
- (33) Juan, Y.; Ke-Qiang, Q. Preparation of activated carbon by chemical activation under vacuum. *Environ. Sci. Technol.* **2009**, 43 (9), 3385–3390.
- (34) Mahvi, A. Application of ultrasonic technology for water and wastewater treatment. *Iran. J. Public Health* **2009**, 38 (2), 1–17.
- (35) Garrido, J.; Linares-Solano, A.; Martin-Martinez, J.; Molina-Sabio, M.; Rodriguez-Reinoso, F.; Torregrosa, R. Use of nitrogen vs. carbon dioxide in the characterization of activated carbons. *Langmuir* 1987, 3 (1), 76–81.
- (36) Thommes, M.; Kaneko, K.; Neimark, A. V.; Olivier, J. P.; Rodriguez-Reinoso, F.; Rouquerol, J.; Sing, K. S. Physisorption of gases, with special reference to the evaluation of surface area and pore size distribution (IUPAC Technical Report). *Pure Appl. Chem.* **2015**, 87 (9–10), 1051–1069.
- (37) Dabrowski, A. Adsorption from theory to practice. *Adv. Colloid Interface Sci.* **2001**, 93, 135–224.
- (38) Houshmand, A.; Wan Daud, W. M. A.; Shafeeyan, M. S. Exploring Potential Methods for Anchoring Amine Groups on the Surface of Activated Carbon for CO₂ Adsorption. *Sep. Sci. Technol.* **2011**, *46* (7), 1098–1112.
- (39) Huang, Z.-H.; Wang, M.; Wang, L.; Kang, F. Relation between the charge efficiency of activated carbon fiber and its desalination performance. *Langmuir* **2012**, 28 (11), 5079–5084.
- (40) Yue, M. B.; Chun, Y.; Cao, Y.; Dong, X.; Zhu, J. H. CO₂ capture by as prepared SBA 15 with an occluded organic template. *Adv. Funct. Mater.* **2006**, *16* (13), 1717–1722.
- (41) (a) Teng, Y.; Li, L.; Xu, G.; Zhang, K.; Li, K. Promoting Effect of Inorganic Alkali on Carbon Dioxide Adsorption in Amine-Modified MCM-41. *Energies* **2016**, 9 (9), 667. (b) Yue, M. B.; Sun, L. B.; Cao, Y.; Wang, Y.; Wang, Z. J.; Zhu, J. H. Efficient CO₂ capturer derived from as synthesized MCM 41 modified with amine. *Chem. Eur. J.* **2008**, *14* (11), 3442–3451.
- (42) Alvis, R. S.; Hatcher, N. A.; Weiland, R. H. CO₂ removal from syngas using piperazine-activated MDEA and potassium dimethyl glycinate. Presented at *Nitrogen+ Syngas*, February 2012, Athens, Greece, 2012; pp 20–23.
- (43) Shah, Y. T.; Pandit, A.; Moholkar, V. Cavitation reaction engineering; Springer Science & Business Media, 2012.

- (44) Sun, K.; Tang, J.; Gong, Y.; Zhang, H. Characterization of potassium hydroxide (KOH) modified hydrochars from different feedstocks for enhanced removal of heavy metals from water. *Environ. Sci. Pollut. Res.* **2015**, 22 (21), 16640–16651.
- (45) Zhou, Y.; Gao, B.; Zimmerman, A. R.; Fang, J.; Sun, Y.; Cao, X. Sorption of heavy metals on chitosan-modified biochars and its biological effects. *Chem. Eng. J.* **2013**, 231, 512–518.
- (46) Ferrari, A. C. Raman spectroscopy of graphene and graphite: disorder, electron—phonon coupling, doping and nonadiabatic effects. *Solid State Commun.* **2007**, *143* (1), 47–57.
- (47) McDonald-Wharry, J.; Ripberger, G.; Manley-Harris, M.; Pickering, K. L. Studying carbonisation with raman spectroscopy. *New Zealand 2013 Biochar Workshop—The Final Answer?*, 2013; pp 16—16
- (48) Perumbilavil, S.; Sankar, P.; Priya Rose, T.; Philip, R. White light Z-scan measurements of ultrafast optical nonlinearity in reduced graphene oxide nanosheets in the 400–700 nm region. *Appl. Phys. Lett.* **2015**, *107* (5), 051104.
- (49) Theodore, M.; Hosur, M.; Thomas, J.; Jeelani, S. Influence of functionalization on properties of MWCNT-epoxy nanocomposites. *Mater. Sci. Eng., A* **2011**, *528* (3), 1192–1200.
- (50) Songolzadeh, M.; Soleimani, M.; Takht Ravanchi, M.; Songolzadeh, R. Carbon dioxide separation from flue gases: a technological review emphasizing reduction in greenhouse gas emissions. *Sci. World J.* **2014**, *2014*, 1.
- (51) Qi, G.; Wang, Y.; Estevez, L.; Duan, X.; Anako, N.; Park, A.-H. A.; Li, W.; Jones, C. W.; Giannelis, E. P. High efficiency nanocomposite sorbents for CO₂ capture based on amine-function-alized mesoporous capsules. *Energy Environ. Sci.* **2011**, *4* (2), 444–452
- (52) Dao, D. S.; Yamada, H.; Yogo, K. Large-pore mesostructured silica impregnated with blended amines for CO₂ capture. *Ind. Eng. Chem. Res.* **2013**, 52 (38), 13810–13817.
- (53) Lu, X.-H.; Sun, Y.-W.; Wei, X.-L.; Peng, C.; Zhou, D.; Xia, Q.-H. Solid base catalyzed highly efficient N-alkylation of amines with alcohols in a solvent-free system. *Catal. Commun.* **2014**, *55*, 78–82.
- (54) Yang, H.; Cui, X.; Dai, X.; Deng, Y.; Shi, F. Carbon-catalysed reductive hydrogen atom transfer reactions. *Nat. Commun.* **2015**, *6*, 6478
- (55) Gebald, C.; Wurzbacher, J. A.; Tingaut, P.; Zimmermann, T.; Steinfeld, A. Amine-Based Nanofibrillated Cellulose As Adsorbent for CO₂Capture from Air. *Environ. Sci. Technol.* **2011**, *45* (20), 9101–
- (56) Zelenak, V.; Halamova, D.; Gaberova, L.; Bloch, E.; Llewellyn, P. Amine-modified SBA-12 mesoporous silica for carbon dioxide capture: Effect of amine basicity on sorption properties. *Microporous Mesoporous Mater.* **2008**, *116* (1), 358–364.
- (57) Plaza, M.; Pevida, C.; Arenillas, A.; Rubiera, F.; Pis, J. CO₂ capture by adsorption with nitrogen enriched carbons. *Fuel* **2007**, *86* (14), 2204–2212.
- (58) Wang, Q.; Luo, J.; Zhong, Z.; Borgna, A. CO₂ capture by solid adsorbents and their applications: current status and new trends. *Energy Environ. Sci.* **2011**, *4* (1), 42–55.
- (59) Chiang, Y.-C.; Chen, Y.-J.; Wu, C.-Y. Effect of Relative Humidity on Adsorption Breakthrough of CO₂ on Activated Carbon Fibers. *Materials* **2017**, *10* (11), 1296.
- (60) Li, L.; Voice, A. K.; Li, H.; Namjoshi, O.; Nguyen, T.; Du, Y.; Rochelle, G. T. Amine blends using concentrated piperazine. *Energy Procedia* **2013**, *37*, 353–369.
- (61) Choi, W.-J.; Seo, J.-B.; Jang, S.-Y.; Jung, J.-H.; Oh, K.-J. Removal characteristics of CO₂ using aqueous MEA/AMP solutions in the absorption and regeneration process. *J. Environ. Sci.* **2009**, *21* (7), 907–913.
- (62) Matthias, M.; Kaneko, K.; Neimark, A. V.; Olivier, J. P.; Rodriguez-Reinoso, F.; Rouquerol, J.; Sing, K. S. W. Physisorption of gases, with special reference to the evaluation of surface area and pore size distribution (IUPAC Technical Report). *Pure Appl. Chem.* **2015**, 87 (9–10), 1051–1069.

(63) Brunauer, S.; Deming, L. S.; Deming, W. E.; Teller, E. On a Theory of the van der Waals Adsorption of Gases. *J. Am. Chem. Soc.* **1940**, 62 (7), 1723–1732.

- (64) Versteeg, G.; van Swaaij, W. P. M. On the kinetics between CO2 and alkanolamines both in aqueous and non-aqueous solutions—I. Primary and secondary amines. *Chem. Eng. Sci.* 1988, 43 (3), 573–585.
- (65) Yue, M. B.; Sun, L. B.; Cao, Y.; Wang, Y.; Wang, Z. J.; Zhu, J. H. Efficient CO₂ capturer derived from as synthesized MCM 41 modified with amine. *Chem. Eur. J.* **2008**, *14* (11), 3442–3451.
- (66) Madzaki, H.; KarimGhani, W. A. W. A.; et al. Carbon dioxide adsorption on sawdust biochar. *Procedia Eng.* **2016**, *148*, 718–725.
- (67) Zhao, Y.; Ding, H.; Zhong, Q. Preparation and characterization of aminated graphite oxide for CO₂ capture. *Appl. Surf. Sci.* **2012**, 258 (10), 4301–4307.
- (68) Kongnoo, A.; Intharapat, P.; Worathanakul, P.; Phalakornkule, C. Diethanolamine impregnated palm shell activated carbon for CO₂ adsorption at elevated temperatures. *J. Environ. Chem. Eng.* **2016**, 4 (1), 73–81.
- (69) Yan, X.; Zhang, L.; Zhang, Y.; Yang, G.; Yan, Z. Amine-Modified SBA-15: Effect of Pore Structure on the Performance for CO₂ Capture. *Ind. Eng. Chem. Res.* **2011**, *50* (6), 3220–3226.
- (70) Hinkov, I.; Lamari, F. D.; Langlois, P.; Dicko, M.; Chilev, C.; Pentchev, I. Carbon dioxide capture by adsorption. *J. Chem. Technol. Metall.* **2016**, *51* (6), 609.
- (71) Xiong, Z.; Shihong, Z.; Haiping, Y.; Tao, S.; Yingquan, C.; Hanping, C. Influence of NH₃/CO₂ modification on the characteristic of biochar and the CO₂ capture. *BioEnergy Res.* **2013**, *6* (4), 1147–1153.
- (72) Bamdad, H.; Hawboldt, K.; MacQuarrie, S. Nitrogen Functionalized Biochar as a Renewable Adsorbent for Efficient CO₂ Removal. *Energy Fuels* **2018**, 32 (11), 11742–11748.